Bis(2,1,3-Benzotelluradiazolidyl) 2,1,3-Benzotelluradiazole: a Pair of Radical Anions Coupled by Te···N Chalcogen Bonding

Nikolay A. Puskarevsky,*[a, b] Anton I. Smolentsev,[a, b] Alexey A. Dmitriev,[c, d] Ignacio Vargas-Baca,*[e] Nina P. Gritsan,[c, d] Jens Beckmann,*[f] and Andrey V. Zibarev*[d, g]

SUPPLEMENTARY INFORMATION

[a] *Dr. N. A. Pushkarevsky, Dr. A. I. Smolentsev*
Nikolaev Institute of Inorganic Chemistry
Siberian Branch of the Russian Academy of Sciences, 630090 Novosibirsk (Russia)
E-mail: nikolay@niic.nsc.ru
[b] *Dr. N. A. Pushkarevsky, Dr. A. I. Smolentsev*
Department of Natural Sciences
Novosibirsk State University, 630090 Novosibirsk (Russia)
[c] *Dr. A. A. Dmitriev, Prof. Dr. N. P. Gritsan*
Voevodsky Institute of Chemical Kinetics and Combustion
Siberian Branch of the Russian Academy of Sciences, 630090 Novosibirsk (Russia)
[d] *Dr. A. A. Dmitriev, Prof. Dr. N. P. Gritsan. Prof. Dr. A. V. Zibarev*
Department of Physics
Novosibirsk State University, 630090 Novosibirsk (Russia)
[e] *Prof. Dr. I. Vargas-Baca*
Department of Chemistry and Chemical Biology
McMaster University, L8S 4M1 Ontario (Canada)
E-mail: vargas@chemistry.mcmaster.ca
[f] *Prof. Dr. J. Beckmann*
Institute for Inorganic Chemistry and Crystallography
University of Bremen, 28359 Bremen (Germany)
E-mail: j.beckmann@uni-bremen.de
[g] *Prof. Dr. A. V. Zibarev*
Vorozhtsov Institute of Organic Chemistry
Siberian Branch of the Russian Academy of Sciences, 630090 Novosibirsk (Russia)
E-mail: zibarev@nioch.nsc.ru

Contents

1. ORCID identification numbers

0000-0001-8668-6362 (N. A. Puskarevsky)
0000-0001-6260-8124 (A. A. Dmitriev)
0000-0002-3074-2051 (I. Vargas-Baca)
0000-0002-2263-1300 (N. P. Gritsan)
0000-0002-8548-1821 (J. Beckmann)
0000-0002-5961-423X (A. V. Zibarev)

2. General

All synthetic experiments were performed under argon using common vacuum-line, Schlenk, sealed ampoule and glove-box techniques. THF was dried by Na-K alloy with benzophenone ketyl and distilled under argon. Compound **3**[1] and KC_8[2] were prepared by known methods, and 18-crown-6 was received from Aldrich. IR spectra were obtained with a Simex FT-801 spectrometer for pellets in KBr prepared in a glovebox. Analyses for C, H and N were performed with CHNS-Analyzer Euro EA 3000.

3. Synthesis

[K(18-crown-6)(THF)]$^+_2$[3$_3$]$^{2-}$. Onto a mixture of **3** (0.150 g, 0.647 mmol), KC_8 (0.086 g, 0.63 mmol) and 18-crown-6 (0.161 g, 0.61 mmol) in a Schlenk tube equipped with greaseless stopcock, 10 mL of THF were transferred via vacuum line at –196 °C. The reaction mixture was slowly warmed-up to 0 °C and stirred for 1 h at this temperature. The resulting dark brown solution was filtered through a fine glass frit, the filtrate evaporated under vacuum to the volume of 2 mL and kept at 4 °C overnight. Dark-brown block-like crystal crystals were separated by decantation, washed with a small amount of THF and carefully dried under vacuum. Salt [K(18-crown-6)(THF)]$^+_2$[**3**$_3$]$^{2-}$ was obtained in the yield of 0.134 g (43% according to the initial amount of **3**). Found, %: C, 40.7; H, 5.4; N, 6.2. Calculated for $C_{50}H_{76}K_2N_6O_{14}Te_3$, %: C, 41.5; H, 5.3; N, 5.8. Slightly lower carbon content can be caused by the partial loss of coordinated THF molecules, *e.g.* for the formula $[K(18\text{-crown-}6)(THF)_{0.75}]^+{}_2[\mathbf{3}_3]^{2-}$ the calculated values are, %: C, 40.9; H, 5.2; N, 6.0. IR, ν, cm^{-1}: 3373 m br, 3274 w sh, 3202 w sh, 3053 w br, 2890 s br, 1628 w, 1593 w, 1504 m, 1487 w, 1424 w, 1351 m, 1284 m, 1250 m, 1108 s, 960 m, 836 w, 743 m, 666 m br, 582 w.

4. X-ray diffraction

XRD study of $[K(18\text{-crown-}6)(THF)]^+{}_2[\mathbf{3}_3]^{2-}$ (Table S1) was performed with a Bruker-Nonius X8 Apex 4K CCD diffractometer using graphite-monochromatized Mo-Kα radiation, λ = 0.71073 Å. The data were collected by the standard technique with φ- and ω-scans of narrow frames. The data reduction and multi-scan absorption were accounted with the *SADABS* program.[3]. The structure was solved by direct methods and refined by full-matrix least-squares on F^2 using the *SHELXL-2018/3* program.[4] All non-hydrogen atoms were refined anisotropically. Hydrogen atoms were placed in calculated positions and refined by using a riding model. The complete crystallographic data have been deposited at the Cambridge Crystallographic data Centre. These can be obtained free of charge from CCDC *via* www.ccdc.cam.ac.uk/structures.

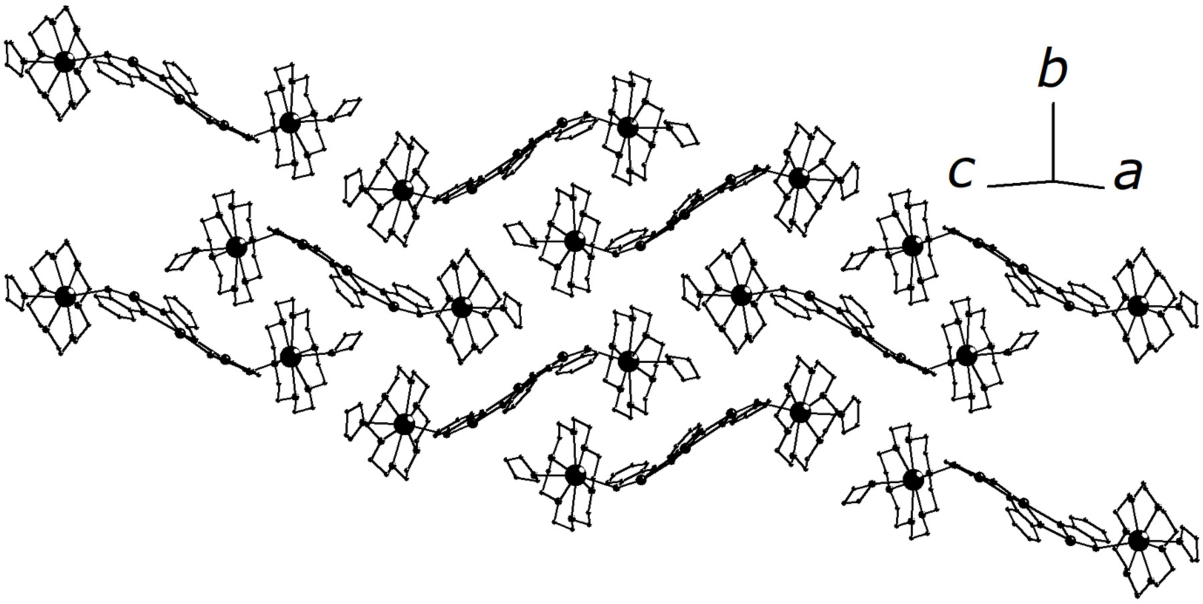

Figure S1. Crystal packing (view perpendicular to a single layer) in the crystal of $[K(18\text{-crown-}6)(THF)]^+{}_2[\mathbf{3}_3]^{2-}$.

Table S1. Crystallographic data for [K(18-crown-6)(THF)]$^{+}_{2}$[**3**$_3$]$^{2-}$

Empirical formula	$C_{50}H_{76}K_2N_6O_{14}Te_3$
Formula weight	1446.16
Temperature (K)	150(2)
Crystal size (mm^3)	0.20 × 0.15 × 0.07
Crystal system	Monoclinic
Space group	*C*2/*c*
Z	8
a (Å)	24.4967(8)
b (Å)	14.9469(5)
c (Å)	32.9263(9)
β (°)	95.3460(10)
V (Å^3)	12003.5(7)
$D_{\text{calcd.}}$ (g cm^{-3})	1.600
μ (Mo Kα) (mm^{-1})	1.651
θ range (°)	1.67 – 27.52
h, k, l indices range	$-31 \le h \le 31$; $-19 \le k \le 19$; $-30 \le l \le 42$
F(000)	5792
Reflections collected	44269
Unique reflections	13398 (R_{int} = 0.0475)
Observed reflections [$I > 2\sigma(I)$]	10058
Parameters refined	676
$R[F^2 > 2\sigma(F^2)]$	$R_1 = 0.0365$, $wR_2 = 0.0601$
$R(F^2)$ (all data)	$R_1 = 0.0670$, $wR_2 = 0.0718$
GOOF on F^2	1.019
$\Delta\rho_{\text{max}}$, $\Delta\rho_{\text{min}}$ (e Å^{-3})	2.314, –1.555
CCDC	1958249

5. Quantum chemical calculations

The electronic structure of the isolated [**3**$_3$]$^{2–}$ in its XRD geometry (neither [K(18-crown-6)(THF)]$^+$ nor K$^+$ cations were taken into account) was calculated at the CASSCF level[5] with the (2,3) and (2,4) active spaces consisting of 2 electrons on 3 (Figure S2) or 4 molecular orbitals, respectively. The DKH2-Hamiltonian[6] was used to account for the scalar relativistic effects, and the ANO-RCC-VDZ[5,7] relativistic basis set was employed. Calculations were performed for the lowest-energy singlet and triplet states of [**3**$_3$]$^{2–}$. To account for the dynamic electron correlation, the CASPT2[8] calculations were performed. The *MOLCAS 8.0* program package[9] was used.

To calculate the triplet-singlet splitting for [**3**$_3$]$^{2–}$ in the XRD geometry, the broken-symmetry (BS)[10] DFT calculations at the UB3LYP level of theory[11] with def2-tzvp basis set[12] (with ECP for Te; 28 core electrons)[13] were carried out. The *ORCA 4.0.1* program package[14] was used.

The geometries of individual **3**, **3**$^{\cdot–}$ and complexes **3**$_2$, [**3**$_2$]$^{\cdot–}$, [**3**$_2$]$^{2–}$ in the singlet and triplet states, and [**3**$_3$]$^{2–}$ in the singlet and triplet states, were optimized in THF solution at the B97-D3 level[15,16] with def2-tzvp basis set with ECP for Te. The influence of the solvent was taken into account using C-PCM model,[17] and the Gibbs free energies of complex formation were calculated.

Additional DFT calculations were performed using the *SCM ADF* package version 2019.103.[18,19] The adiabatic local density approximation (ALDA) was used for the exchange-correlation kernel, and the differentiated static LDA expression was used with the Vosko-Wilk-Nusair parameterization. The calculations of model geometries were gradient corrected with the exchange and correlation PBE functional.[20] These preliminary geometries were further refined using the hybrid B3LYP functional.[21] However, the N2–N3–N4–N5 torsion potential was only calculated with PBE for computational expediency. All calculations were performed using all-electron triple-ζ basis sets with two polarization functions and applying the zeroth-order relativistic approximation (ZORA)[22] with the specially adapted basis sets and Grimme's D3 dispersion correction.[16]

Results of calculations are presented in Figures S2-S12 and Tables S2 and S3.

Figure S2 displays the MOs of the active space employed for the calculation of the first excited triplet state of [**3**$_3$]$^{2–}$ in XRD geometry. It is seen that each active MO is mainly localized on a specific molecular unit of [**3**$_3$]$^{2–}$, *e.g.* MO1 is localized on unit 2 with slight delocalization onto unit 3, and MO2 on unit 3 with slight delocalization onto unit 2, whereas MO3 is localized almost exclusively on unit 1. The wave function of the lowest-energy triplet state is described exactly by one configuration with MO1 and MO2 occupied by one electron (–21382.77698739 H). Thus, it is clear that spin populations of units 2 (~0.97) and 3 (~1.02) are close to 1, and unit 3 (~0.01) to zero. With both Mulliken (M) and LoProp (L) approaches, the negative charge of [**3**$_3$]$^{2–}$ is noticeably delocalized from unit 2 onto unit 1 (q_1(M) = –0.28; q_1(L) = –0.33). The charge on unit 3 is close to –1 (q_3(M) = –0.97;

$q_3(L) = -0.98$). Account of dynamic electron correlation leads to only minor changes of the charge distribution as Mulliken charges are −0.28, −0.75 and −0.97 for units 1-3, respectively.

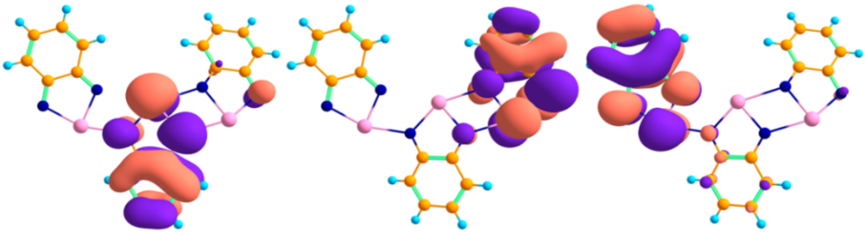

Figure S2. MOs of $[\mathbf{3}_3]^{2-}$ involved in the (2,3) active space for the CASSCF calculations of the triplet state properties.

The CASSCF (2,3) calculations for $[\mathbf{3}_3]^{2-}$ in the singlet state leads to active MOs (Figure S3) which differ from those of triplet state calculation (Figure S2). With Figure S3 it is seen that all three orbitals are localized on units 2 and 3. Besides, the sum and difference of MO1 and MO2 are similar to the MO1 and MO2 from the calculations of the triplet state. All attempts to obtain with orbital rotations and level shifts the same active space as for the triplet state (Figure S2) failed. Therefore, calculations with a larger active space (2,4) MOs (Figure S4) were performed.

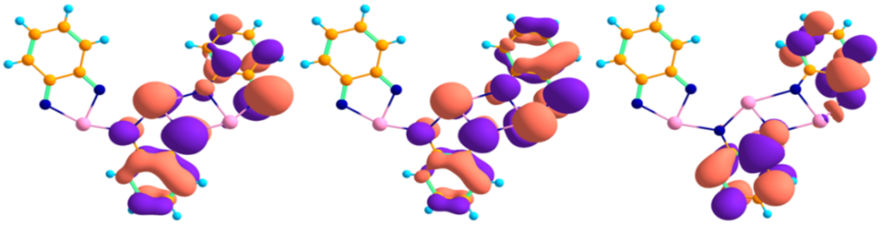

Figure S3. MOs of $[\mathbf{3}_3]^{2-}$ involved in the (2,3) active space for the CASSCF calculations of the singlet state properties.

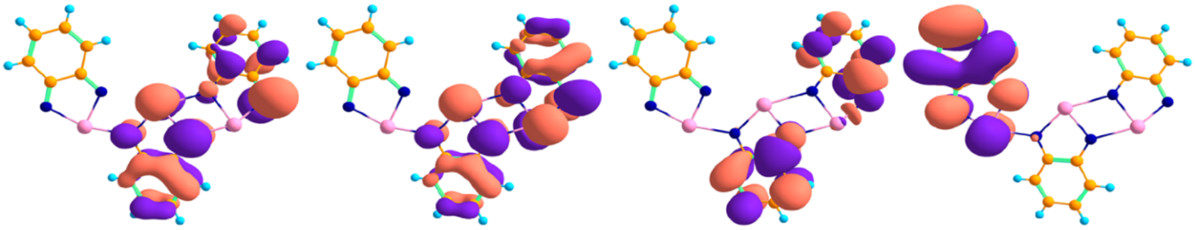

Figure S4. MOs of $[\mathbf{3}_3]^{2-}$ involved in the (2,4) active space for the CASSCF calculations of the singlet state properties.

With Figure S4 it is seen that MO4 of the (2,4) active space is equal to MO3 from calculations of the triplet state (Figure S2). Calculations with both (2,3) and (2,4) active spaces gave the same results. The electronic energies are equal within 3×10^{-7} H (2×10^{-4} kcal·mol^{-1}), and both singlet-state wave functions are described by the difference of two configurations with MO1 and MO2 occupied by two electrons (with 0.725 and 0.275 weight, respectively), the occupation numbers of the natural orbitals are ~1.45 and ~0.55. Note, that both MO1 and MO2 are localized on units 2 and 3. Therefore, the singlet ground state wave function corresponds to almost equal sum of closed-shell (45%) and open-shell diradical (55%) configurations. Overall, with the CASSCF calculations, $[\mathbf{3}_3]^{2-}$ in asymmetric XRD geometry can be assigned as a complex of a neutral **3** (unit 1) with $[\mathbf{3}_2]^{2-}$ (units 2 and 3) in the singlet ground state, *i.e.* featuring only a partial diradical character.

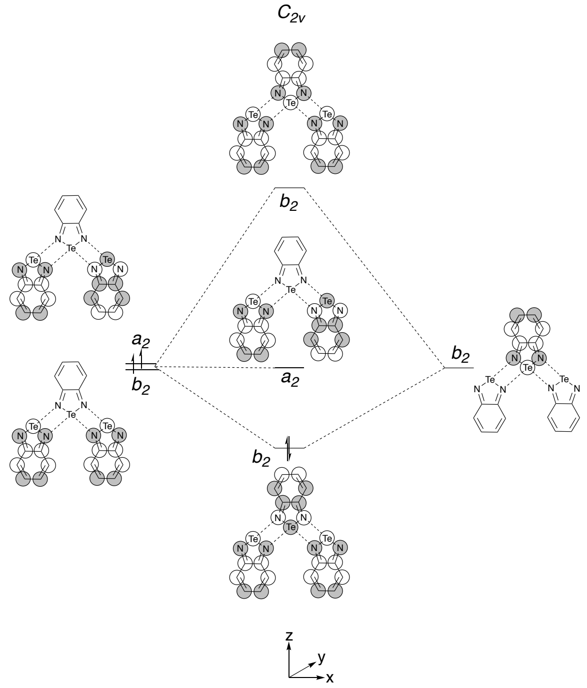

Figure S5. Orbital interactions for the coupling of spins in C_{2v}-idealized $[\mathbf{3}_3]^{2-}$.

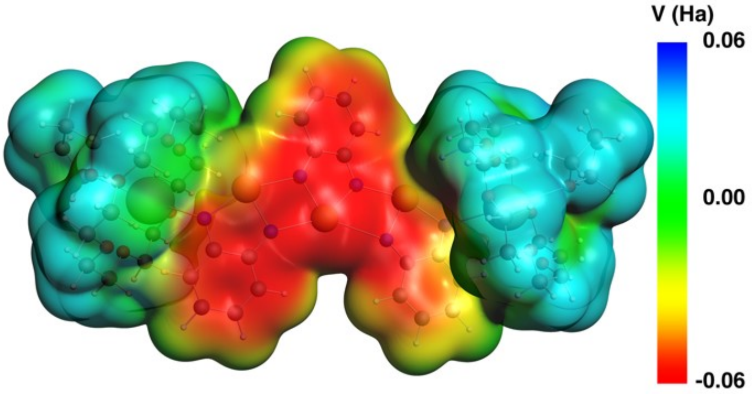

Figure S6. Electrostatic potential map plotted over the 10^{-3} a.u. isodensity surface calculated for $[\mathrm{K(18\text{-}crown\text{-}6)(THF)}]^{+}_{2}[\mathbf{3}_3]^{2-}$. Only the position of the hydrogen atoms is optimized from the crystallographic coordinates.

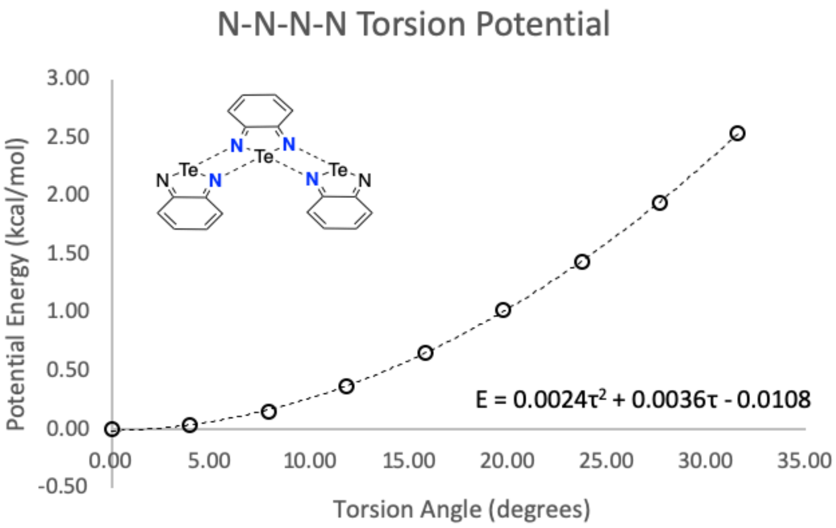

Figure S7. The N–N–N–N torsion potential calculated for [**3**$_3$]$^{2-}$ at the PBE-D3 level.

Table S2. Electron density (ρ) and its Laplacian ($\nabla^2\rho$) at the bond critical point of the [**3**$_3$]$^{2-}$ model calculated (B3LYP-D3, ZORA, TZ2P) at the bond critical points of the Te···N chalcogen bonding interactions.

Interaction	d (Å) Experimental	Calculated C_{2v}	C_s	ρ (e Å^{-3} × 10^2)	$\nabla^2\rho$ (e Å^{-5} × 10^2)
Te1···N3	2.250(3)	2.301	2.304	8.05	13.44
Te2···N2	2.904(3)	2.702	2.731	2.08	5.86
Te2···N5	2.385(3)	2.702	2.663	5.83	12.26
Te3···N4	2.313(3)	2.301	2.304	6.97	12.70

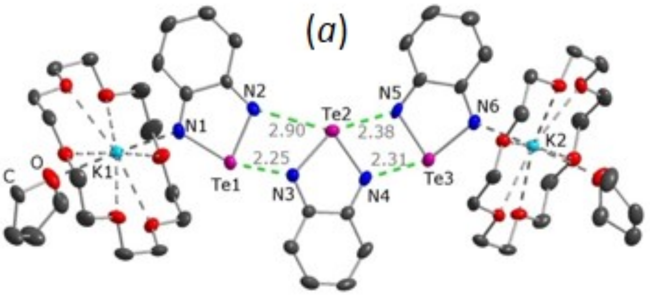

Figure S8 (Figure 1a of main text). XRD molecular structure of salt [K(18-crown-6)(THF)]$^+_2$[**3**$_3$]$^{2-}$ (thermal ellipsoids at 50% probability).

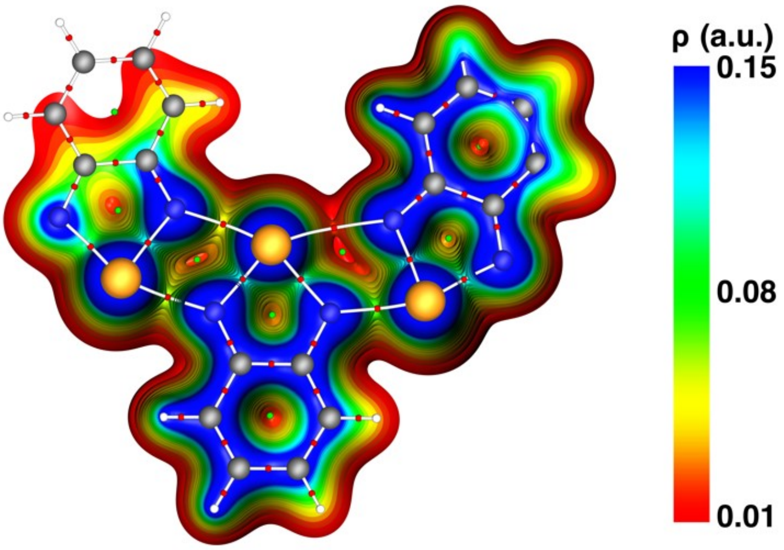

Figure S9. B3LYP-D3-calculated electron density for a $[\mathbf{3}_3]^{2-}$ model in which only the hydrogen atom coordinates are optimized from the crystallographic determination (Figure S8). Iso-surfaces are plotted within the range 0.01-0.15 a.u. and clipped at the plane defined by the tellurium atoms. Atom sphere models, bond paths and critical points are overlaid.

Table S3. DFT (PBE-D3-TZ2P-ZORA) Energy Decomposition Analysis (kcal mol^{-1}) calculated using the transition state method[23] for optimized aggregates of **3** and $\mathbf{3}^{\cdot-}$.

	$\mathbf{3} \cdots \mathbf{3}$	$\mathbf{3}^{\cdot-} \cdots \mathbf{3}^{\cdot-}$	$\mathbf{3}^{\cdot-} \cdots \mathbf{3}^{\cdot-}$	$\mathbf{3} \cdots \mathbf{3}^{\cdot-}$	$\mathbf{3}^{\cdot-} \cdots \mathbf{3} \cdots \mathbf{3}^{\cdot-}$
Interactions	$[\mathrm{Te\text{-}N}]_2$	π-π^{c}	$[\mathrm{Te\text{-}N}]_2$	$[\mathrm{Te\text{-}N}]_2$	$[\mathrm{Te\text{-}N}]_2 \times 2$
E_{Pauli}	92.2	6.4	201.9	193.6	304.3
$E_{Electrostatic}$	-65.1	59.1	-76.2	-128.0	-160.3
$E_{Steric}{}^{a}$	27.1	65.6	125.7	65.5	144.0
$E_{Orbital}$	-45.1	-8.6	-100.5	-107.5	-173.1
$E_{Dispersion}$	-2.7	-4.0	-2.8	-2.8	-6.0
$E_{Total}{}^{b}$	-20.7	53.0	22.4	-44.8	-35.1

a) $E_{Steric} = E_{Electrostatic} + E_{Pauli}$

b) $E_{Total} = E_{Steric} + E_{Orbital} + E_{Dispersion}$

c) face-to-face dimer, 1.7° angle between molecular planes, d(Te---Te) = 4.14 Å; d(C---C)Avg = 4.32 Å.

Figures S10-S12 show optimized geometries of **3**, $\mathbf{3}^{\cdot-}$ and their complexes including $[\mathbf{3}_3]^{2-}$ in THF solution. The longest Te···N distance of 2.682 Å is observed for $\mathbf{3}_2$. In $[\mathbf{3}_2]^{\cdot-}$ this distance is shortened to 2.469 Å, and in singlet $[\mathbf{3}_2]^{2-}$ to 2.367 Å. However, in triplet $[\mathbf{3}_2]^{2-}$ the Te…N distance of ~2.690 Å is close to that in $\mathbf{3}_2$ (Figures S10 and S11). Optimized geometries of $[\mathbf{3}_3]^{2-}$ in the singlet and triplet state are close to the C_S symmetry (Figure S12). The ground singlet-state geometry is characterized by two short Te···N distances of 2.314 Å which are similar to those in $[\mathbf{3}_2]^{2-}$ in the singlet state, and by two longer distances of ~2.64 Å which are close to the distance in $\mathbf{3}_2$. In the excited triplet state of $[\mathbf{3}_3]^{2-}$, the shorter distances get significantly elongated to ~2.49 Å approaching those in $[\mathbf{3}_2]^{\cdot-}$, while the longer distances remain practically intact (~2.66 Å).

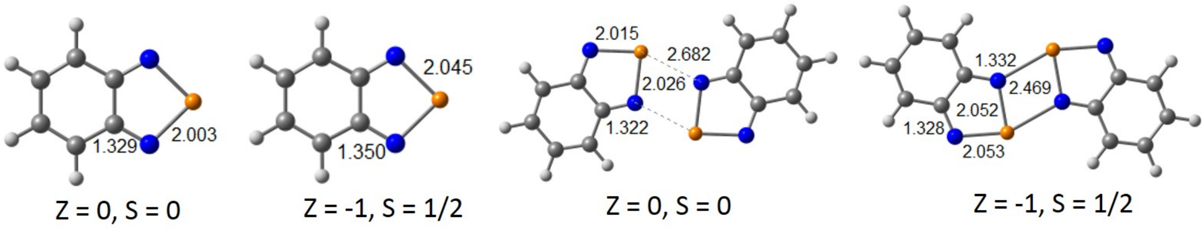

Figure S10. B97-D3-Optimized structures of **3** (Z = 0, S = 0), $\mathbf{3}^{\cdot-}$ (Z = –1, S = ½), $\mathbf{3}_2$ (Z = 0, S = 0) and $[\mathbf{3}_2]^{\cdot-}$ (Z = –1, S = ½) in THF solution.

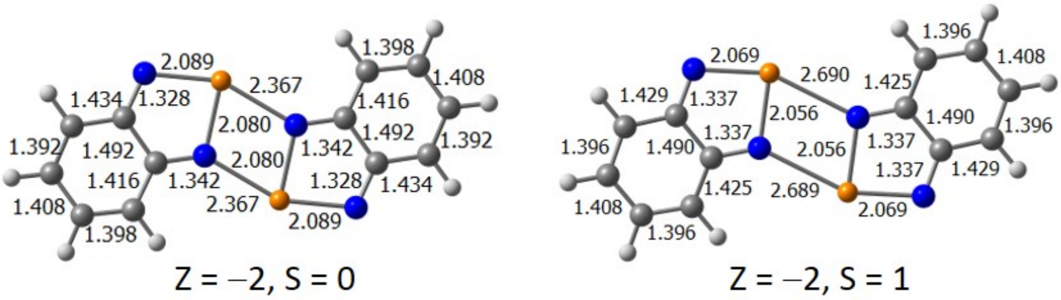

Figure S11. B97-D3-Optimized structures of $[\mathbf{3}_2]^{2-}$ in the ground singlet (S = 0) and excited triplet (S = 1) states in THF solution.

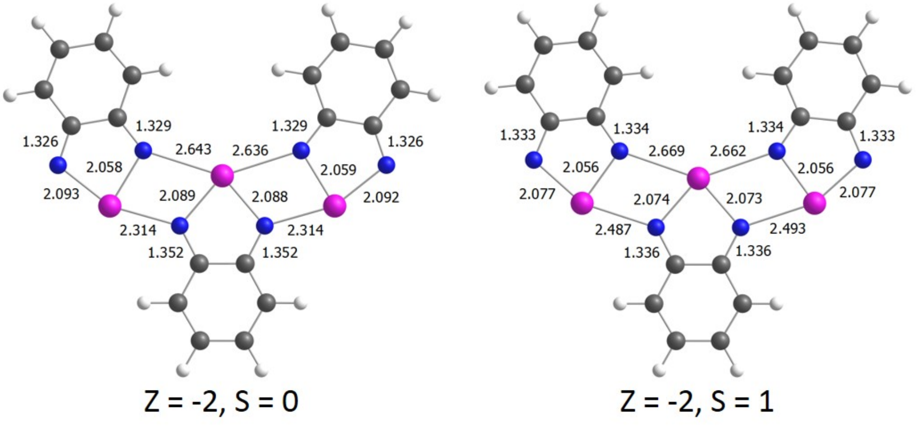

Figure S12. B97-D3-Optimized structures of $[\mathbf{3}_3]^{2-}$ in the ground singlet (S = 0) and excited triplet (S = 1) states in THF solution.

6. Electron paramagnetic resonance

EPR spectra were measured with a Bruker ELEXSYS-II E500/540 spectrometer (X-band, MW frequency 9.8689 GHz, MW power of 20 mW, modulation frequency of 100 kHz, and modulation amplitude of 0.006 mT) equipped with a high-Q cylindrical resonator ER4119HS. Solution spectra of [K(18-crown-6)(THF)]$^{+}_{2}$[**3**$_{3}$]$^{2-}$ were collected for freshly prepared solutions in absolute 2-methyltetrahydrofuran (~10^{-3} M), the samples were flame-sealed.

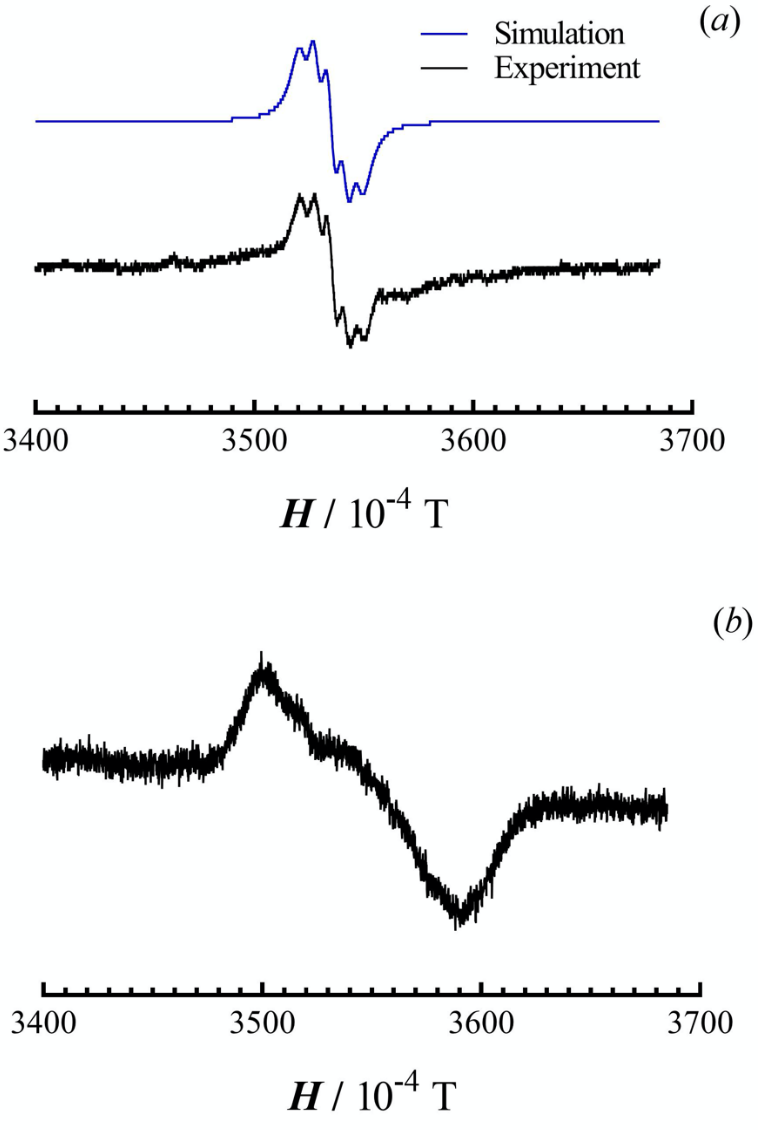

Figure S13. (a) EPR spectrum of a solution of [K(18-crown-6)(THF)]$^{+}_{2}$[**3**$_{3}$]$^{2-}$ in THF under anaerobic conditions and room temperature. The spectrum is identical to the spectrum of **3**$^{-}$ in reference 1. (b) EPR spectrum of crystalline [K(18-crown-6)(THF)]$^{+}_{2}$[**3**$_{3}$]$^{2-}$ at room temperature. Paramagnetic admixture quantified by the Absolute-Spin method would correspond to 0.4% of the **3**$^{-}$ units in the crystal. However, given the large singlet-triplet gap [**3**$_{3}$]$^{2-}$, the paramagnetism is likely due to minute amounts of uncoupled **3**$^{-}$ or defects of the crystal lattice.

7. SQUID magnetometry

Magnetic measurements on $[\text{K(18-crown-6)(THF)}]^{+}_{2}[3_{3}]^{2-}$ were performed with a Quantum Design MPMS XL SQUID magnetometer in the temperature range 2-300 K. The sample was sealed in a weighed polyethylene cap inside a glovebox.

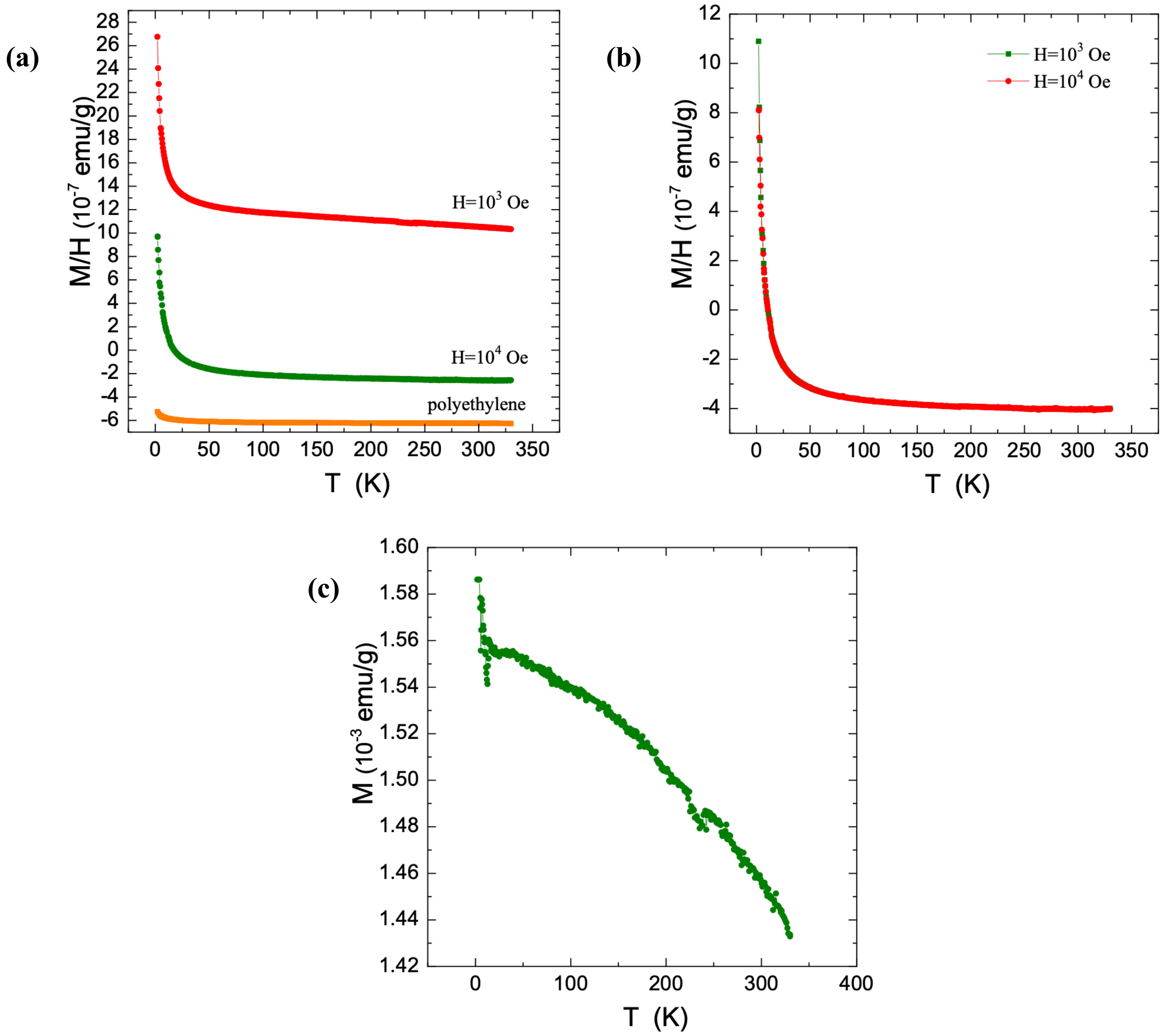

Figure S14. SQUID measurements for crystalline $[\text{K(18-crown-6)(THF)}]^{+}_{2}[\mathbf{3}_{3}]^{2-}$. (a) Raw susceptibility measurements for sample and packaging. The effect of a very weak ferromagnetic contribution (it saturates with the field and does not depend on the temperature) from an impurity (ca. 1 ppm) is noticeable. (b) Susceptibility after correction for the ferromagnetic contribution. (c) Ferromagnetic contribution of said impurity.

8. References

[1] N. A. Pushkarevsky, E. A. Chulanova, L. A. Shundrin, A. I. Smolentsev, G. E. Salnikov, E. A. Pritchina, A. M. Genaev, I. G. Irtegova, I. Yu. Bagryanskaya, S. N. Konchenko, N. P. Gritsan, J. Beckmann, A. V. Zibarev, *Chem. Eur. J.* **2019**, *25*, 806–816.

[2] W. A. Herrmann, C. Zybill, in: *Synthetic Methods of Organometallic and Inorganic Chemistry,* Vol. 1, Eds. W. A. Herrmann, A. Salzer, Georg Thieme: Stuttgart, 1999.

[3] *Bruker Advanced X-ray Solutions*, *APEX2* (Version 1.08), *SAINT* (Version 7.03), SADABS (Version 2.11), Bruker AXS Inc., Madison, WI, USA, **2004**.

[4] G. M. Sheldrick, *Acta Crystallogr. C* **2015**, *71*, 3–8.

[5] a) F. Aquilante, L. De Vico, N. Ferre, G. Ghigo, P.-A. Malmqvist, P. Neogrady, T. B. Pedersen, M. Pitonak, M. Reiher, B. O. Roos, L. Serrano-Andres, M. Urban, V. Veryazov, R. Lindh, *J. Comput. Chem*. **2010**, *31*, 224247; b) P.-A. Malmqvist, B. O. Roos, *Chem. Phys. Lett*. **1989**, *155*, 189−194; c) B. O. Roos, in *Ab initio methods in quantum chemistry*, Part II, Vol. 69 (Ed: K. P. Lawley), Wiley, N. Y. 1987.

[6] B. A. Hess, *Phys. Rev. A* **1986**, *33*, 3742−3748.

[7] a) K. Andersson, B. O. Roos, *Chem. Phys. Lett*. **1992**, *191*, 507−514; b) K. Pierloot, *Mol. Phy*s. **2003**, *101,* 2083−2094; c) B. O. Roos, K. Andersson, M. P. Felscher, P.-A. Malmqvist, L. Serrano-Andres, K. Pierloot, M. Merchan in *Advanced Chemical Physics*, Vol. 93 (Eds.: I. Prigogine, S. A. Rice), Wiley, Hoboken, 1996, p. 219.

[8] a) K. Andersson, P.-A. Malmqvist, B. O. Roos, A. J. Sadlej, K. Wolinski, *J. Phys. Chem*. **1990**, *94*, 5483−5488; b) K. Andersson, P. Malmqvist, B. O. Roos, *J. Chem. Phys*. **1992**, *96*, 1218−1226.

[9] a) B. O. Roos, R. Lindh, P.-A. Malmqvist, V. Veryazov, P. O. Widmark, *J. Phys. Chem. A* **2004**, *108*, 2851−2858; b) B. O. Roos, R. Lindh, P.-A. Malmqvist, V. Veryazov, P. O. Widmark, *J. Phys. Chem. A* **2005**, *109*, 6575−6579.

[10] a) H. Nagao, M. Nishino, Y. Shigeta, T. Soda, Y. Kitagawa, T. Onishi, Y. Yoshika, K. Yamaguchi, *Coord. Chem. Rev*. **2000**, *198*, 265–295; b) L. Noodleman, D. A. Case, J. M. Mouesca, *Coord. Chem. Rev*. **1995**, *144*, 199–244; c) L. Noodleman, *J. Chem. Phys*. **1981**, *74*, 5737–5743.

[11] a) A. D. Becke, *J. Chem. Phys*. **1993**, *98*, 5648–5652; b) C. Lee, W. Yang, R. G. Parr, *Phys. Rev. B* **1988**, *37*, 785–789.

[12] F. Weigend, R. Ahlrichs, *Phys. Chem. Chem. Phys*. **2005**, *7*, 3297–3305.

[13] a) M. Dolg, H. Stoll, H. Preuss, *J. Chem. Phys.* **1989**, *90*, 1730–1734; b) K. A. Peterson, D. Figgen, E. Goll, H. Stoll, M. Dolg, *J. Chem. Phys*. **2003**, *119*, 11113–11123.

[14] F. Neese, *WIREs Comput. Mol. Sci.* **2018**, *8*, e1327.

[15] S. Grimme, J. Antony, S. Ehrlich, H. Krieg, *J. Chem. Phys*. **2010**, *132*, 154104.

[16] S. Grimme, S. Ehrlich, L. Goerigk, *J. Comput. Chem*. **2011**, *32*, 1456–1465.

[17] V. Barone, M. Cossi, *J. Phys. Chem. A* **1998**, *102*, 1995–2001.

[18] G. te Velde, F. M. Bickelhaupt, E. J. Baerends, C. Fonseca Guerra, S. J. A. van Gisbergen, J. G. Snijders, T. Ziegler, *J. Comp. Chem.* **2001**, *22*, 931–967.

[19] C. F. Guerra, J. G. Snijders, G. te Velde, E. J. Baerends, *Theor. Chem. Acc.* **1998**, *99*, 391–403.

[20] J. P. Perdew, K. Burke, M. Ernzerhof, *Phys. Rev. Let.* **1996**, *77*, 3865–3868.

[21] P. J. Stephens, F. J. Devlin, C. F. Chabalowski, M. J. Frisch, *J. Phys. Chem*. **1994**, *98*, 11623–11626.

[22] a) E. van Lenthe, R. van Leeuwen, E. J. Baerends, J. G. Snijders, *Int. J. Quantum Chem.* **1996**, *57*, 281–293; b) E. van Lenthe, J. G. Snijders, E. J. Baerends, *J. Chem. Phys.* **1996**, *105*, 6505–6516.

[23] a) T. Ziegler, A. Rauk, *Inorg. Chem.* **1979**, *18*, 1558-1565; b) a) T. Ziegler, A. Rauk, *Inorg. Chem.* **1979**, *18*, 1755-1759.